Tunable laser light

Optical cavity containing gas sample

Rapidly swept laser frequency or cavity length

CRD signals

... reflected   ... transmitted

FROM BRIAN J. ORR and YABAI HE, PAGES 1–20, IN THIS ISSUE.

www.elsevier.com/locate/cplett

Contents lists available at ScienceDirect

Chemical Physics Letters

Effect of surface stresses on CuO nanowire growth in the thermal oxidation of copper

Rediola Mema [a], Lu Yuan [a], Qingtian Du [b], Yiqian Wang [b], Guangwen Zhou [a,*]

[a] Department of Mechanical Engineering & Multidisciplinary Program in Materials Science and Engineering, State University of New York, Binghamton, NY 13902, USA
[b] The Cultivation Base for State Key Laboratory, Qingdao University, No. 308 Ningxia Road, Qingdao 266071, China

ARTICLE INFO

ABSTRACT

By exerting bending stresses on a metal surface, we show that in-plane tensile stresses can effectively promote CuO nanowire (NW) formation by significantly increasing the NW growth density during the oxidation of copper. It is found that the improved NW growth is associated with decreased size of oxide grains and increased number of grain boundaries in the underlying Cu_2O and CuO layers. These results are attributed to the effect of in-plane tensile stresses that result in fine grain structures in the underlying oxide layers, which facilitates the outward diffusion of Cu ions for enhanced oxide NW growth.

© 2011 Elsevier B.V. All rights reserved.

1. Introduction

Nanostructured semiconductor materials such as Si, Ge etc. and oxides such as CuO, ZnO, SnO_2, etc. have been the focus of intensive studies due to their emerging and increasing use in nanodevices and integrated nanosystems [1]. Nanowires (NWs) are one-dimensional nanocrystals with large aspect ratio (length/diameter) and have shown unique properties that are tunable by varying size. Most of the ways used to generate oxide nanowires are physical and chemical routes such as precursor methods [2], hydrothermal reaction [3], anodization [4], electrospinning [5], and seed-mediated growth solution [6]. Compared to their relatively complex and multi-step synthesis procedures, the formation of CuO NWs by direct thermal oxidation of metals has been recently given considerable attention due to its simplicity and large-scale growth capability [1,7–22]. Also, oxide NWs prepared by thermal oxidation exhibit higher crystallinity and longer aspect ratios compared to those prepared via solution-based routes [23].

Oxide whisker generation from thermal oxidation dates back to the 1950's [24,25], but the growth mechanism has widely been debated and lacks cohesive understanding [8–10]. With powerful microscopy techniques widely available today, a general consensus established is that the oxidation of metals to form oxide NWs typically requires the sequent growth of multiple and parallel oxide layers (with different oxide phases) followed by the subsequent growth of oxide NWs on the top oxide layer [8,26–31]. While oxide layering can be understood from thermodynamic equilibrium analysis, the growth of oxide NWs is usually attributed to kinetic origins, largely because oxide NWs and the top oxide layer have the same oxide phase and crystal structure [8,27,28].

Due to the large differences in molar volumes between the various oxide phases and the metal substrate, it has been inferred that the presence of interfacial stresses has a substantial effect on the oxide NW formation by promoting grain boundary diffusion for initiating the nucleation and uniaxial growth of oxide NWs on the outmost surface. To date, however, there has been no straightforward experimental verification of this hypothesis. In this Letter we provide such verification in form of results of simple experiments in which in-plane stresses are imposed upon oxidizing metal surfaces. Our results demonstrate unequivocal effects of applied tensile stress on both, the microstructures of the oxide films and the resulting oxide NW growth. This work also provides a simple approach for efficiently promoting oxide nanowire formation by thermal oxidation of metals.

To observe the effects of surface stress, bending is commonly used to apply stress. A schematic of the scenario is shown in Figure 1. As bending occurs, the upper surface is no longer parallel to the bottom surface as the upper face shortens by dL while the bottom face is elongated by dL, causing the generation of compressive stress in the upper face and tension stress in the bottom face. It follows that there is a line or region of zero stress between the two surfaces, called the neutral axis. The amount of bending stress existent at the surfaces can be calculated using the flexure formula of $\sigma = \pm \frac{Ec}{\rho}$, where E is the elastic modulus of the material, c is the position along the vertical direction where the stress is being measured, and ρ is the radius of curvature. An advantage of using bending metals is that the effects of both compressive and tensile stresses can be studied simultaneously by examining oxide NW formation on the upper and bottom face of the bent metal oxidized under the same oxidation conditions. Our hypothesis is that these exerted surface stresses would modify the microstructures of the multilayered oxide films, whereby influencing the mass transport process leading to the nucleation and growth of oxide NWs.

* Corresponding author. Fax: +1 607 777 4620.
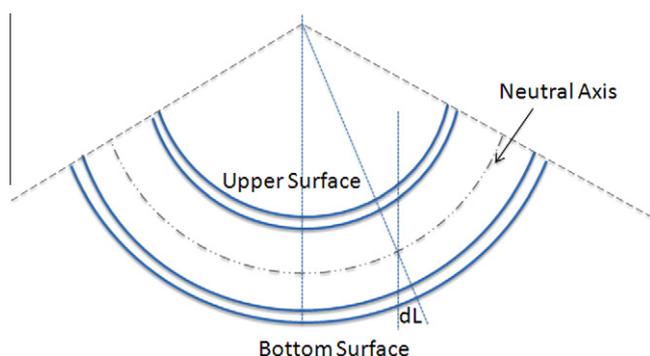 *E-mail address:* gzhou@binghamton.edu (G. Zhou).

Figure 1. Schematic diagram showing the generation of stresses at the upper and bottom surfaces of the sample as induced by uniform bending.

2. Experimental procedure

The test specimens were Cu foils (99.99% purity) with a thickness of 0.25 mm. The foils were cut into strips 5 mm in width and 25 mm in length, following which they were uniformly bent at a radius of 10 mm. The sample was then cleaned with 0.1 M HCl, thoroughly rinsed with deionized water and then put in acetone for an ultrasound bath for 5 min to remove impurities and native oxide from the surface of the metal. The sample was dried in N_2 and then put into an oxidation chamber. The chamber was subsequently pumped to $\sim 10^{-6}$ Torr, oxygen gas was then admitted into the chamber to the pressure of 200 Torr. The samples were then heated up to a temperature of 450 °C at the rate of 10 °C/min in oxygen and then oxidized for 30 min in static oxygen. The oxygen pressure in the chamber increased to at ~ 210 Torr after the sample was heated to the oxidation temperature of 450 °C. The sample temperature is monitored via a K-type thermocouple in contact with the heater. The sample was then cooled down to room temperature (23 °C) at the same rate in oxygen. The oxidation loading apparatus was large enough so that both bent and flat specimens could be loaded simultaneously and then oxidized under the same oxidation conditions. Surface morphology is examined using a field emission scanning electron microscope (FEG-SEM) FEI Supra 55VP. Density of nanowires on the inner and outer surface of the sample was compared to the density of nanowires on the flat sample. The thickness of the oxide layers, size and shape of the oxide grains for the samples was investigated by SEM. The morphology and microstructure of individual CuO NWs are analyzed by transmission electron microscopy (TEM) using a JEOL JEM2100F operated at 200 kV.

3. Experimental results

Both the upper and bottom surfaces (under compressive and tensile stress, respectively, as shown in Figure 1) of the bent Cu foil turn black in color after the oxidation treatment, suggesting that the surface oxide is CuO. Figure 2 shows representative SEM

images of the growth morphology of CuO NWs on the upper and bottom surfaces, respectively. For comparison, an SEM image from the oxidation of unbent (i.e., flat) Cu surface is also given. It can be seen that the bottom surface is covered by dense CuO NWs with a much higher number density than the other two surfaces. The average density of NWs on the bottom surface of the bent Cu is about $5.15/\mu m^2$, while the densities for the upper surface of the bent Cu and flat Cu are $1.23/\mu m^2$ and $1.08/\mu m^2$, respectively. The diameters of CuO NWs grown on these surfaces show no noticeable difference and are all in the range of 40–100 nm. The observations reveal evidently that in-plane tensile stresses (the bottom surface of the bent Cu) result in significantly increased number density of CuO NWs as compared to the compressed or flat Cu.

The lengths of CuO NWs do not show significant dependence on the tensile stresses. Figure 3 shows SEM images from the different surfaces. The lengths of NWs in all images are on average around 4 μm and NWs on the upper and bottom surfaces of the bent Cu and the flat Cu show no obvious difference. TEM analysis of CuO NWs formed on these different surfaces reveals the existence of a bi-crystalline structure in the NWs. The bi-crystalline structure is observed to run along the entire axial direction. As shown in Figure 4a, the NW is divided by a twin boundary, where the different crystal orientations cause visible contrast in the bright-field TEM image. Figure 4b shows a typical selected area electron diffraction (SAED) pattern taken along [1 1 0] zone axis of a single CuO NW. The diffraction pattern can be identified as consisting of two sets of diffraction spots with mirror symmetry, consistent with the nature of the bicrystalline structure within the nanowire. Figure 4c is a high-resolution TEM image confirming the bicrystalline structure of the NW. It can be seen that each side of the twin boundary shows well-developed crystal lattice planes.

In line with previous studies [8,26,27], the formation of CuO NWs on all these Cu surfaces involves Cu_2O/CuO double layer growth with Cu_2O being the bottom layer and CuO being the top layer. However, the microstructure of the underlying oxide layers is observed to show dependence on the type of applied stresses. Figure 5 shows representative cross-sectional SEM images of CuO/Cu_2O layers on the bent and unbent Cu. For all the cases, the Cu_2O bottom layers contain column like grains while the CuO intermediate layer consists of finer grains. Several features can be noted from their comparison. In the case of tensile stress the average sizes of Cu_2O and CuO grains are smaller than that of oxide grains affected by compressive stress or flat sample. In addition, both the Cu_2O and CuO layers have larger thickness for the tensile stress case than that of compressive stresses or flat Cu. Their quantitative comparison is listed in Table 1, where the oxide grain sizes are estimated from cross-sectional SEM images by measuring the lateral sizes of individual grains. Measurements performed on samples cut along different directions were used for better statistics. The uncertainty numbers given in Table 1 correspond to the range of variation of the quantities measured from the different sample areas. The thickness of oxide layers and sizes of oxide grains vary differently with the various sample areas examined, different uncertainties are therefore obtained for these quantities.
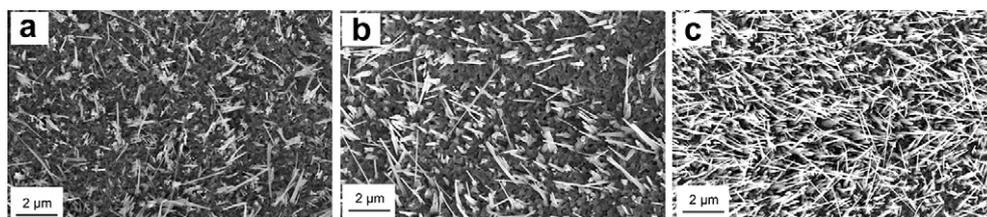

Figure 2. SEM images of the oxide surface for (a) unbent Cu, (b) upper surface of the bent Cu, and (c) bottom surface of the bent Cu.
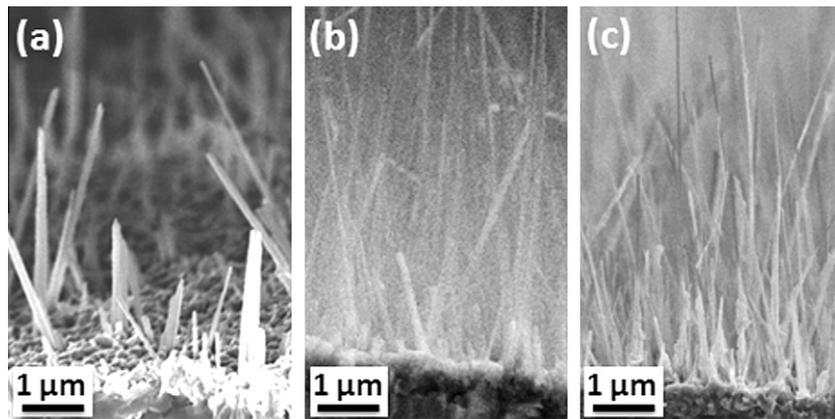
Figure 3. Cross-sectional SEM images of CuO NWs grown on different surfaces, (a) unbent Cu, (b) upper surface of bent Cu, (c) bottom surface of bent Cu.
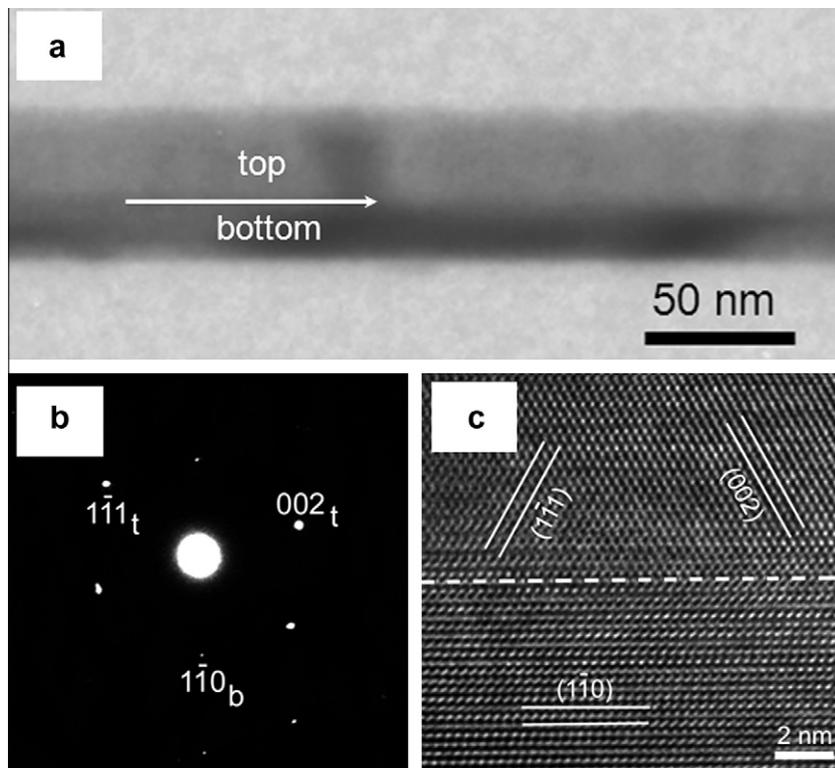

Figure 4. (a) The contrast from a BF TEM image of an individual CuO NW suggests the presence of a twin boundary along the axial direction of the NW. (b) SAED pattern obtained from a single NW. Indices with subscript 'b' refer to the bottom side of the NW shown in (a), indices with subscript 't' refer to the top side. (c) HRTEM image of the NW showing the twin boundary of the NW.
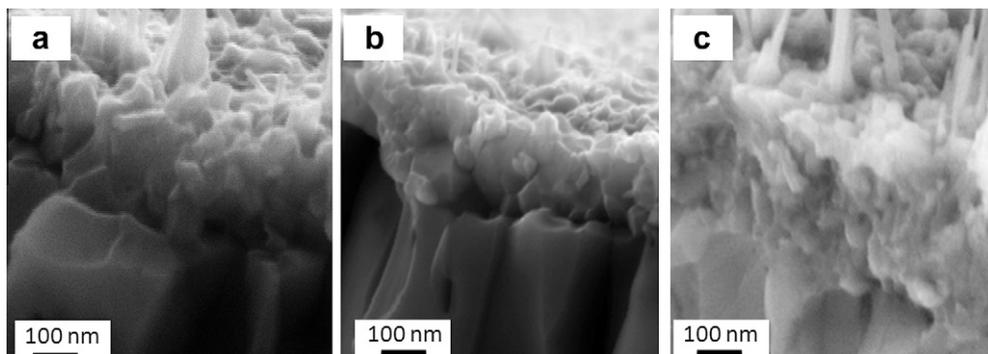

Figure 5. Cross-sectional SEM images of the oxide layers and oxide grain morphologies for (a) unbent Cu, (b) upper surface of bent Cu, and (c) bottom surface of bent Cu.

Table 1
Tabulated data for each of the cases studied: flat surface, bent Cu (upper and bottom).

	Nanowire density (1/μm^2) (±0.1)	Cu_2O layer (μm)		CuO layer (μm)	
		Thickness (±0.2)	Grain Size (±0.05)	Thickness (±0.05)	Grain Size (±0.02)
Flat Cu	1.08	3	0.45	0.2	0.1
Bent Cu					
Upper surface (Compressive stress)	1.23	2.7	0.4	0.2	0.12
Bottom surface (Tensile stress)	5.15	3.7	0.1	0.4	0.05

Similar to the effect of CuO NW density, the effect of tensile stress on the oxide growth is noticeable, i.e., decreasing the average sizes of Cu_2O and CuO grains and increasing the average thickness of the Cu_2O and CuO layers. However, the case of compressive stress does not show obvious difference in comparison to the flat Cu sample.

4. Discussion

Table 1 summarizes the results of the experimental measurements on the different samples. The differences in the NW densities, grain size and thickness of Cu_2O and CuO layer between the upper surface (under compressive stress) of the bent sample and flat Cu (stress-free surface) is small and at variance, and no definite conclusion can be drawn. However, one clear trend is evident: in-plane tensile stresses (i.e., the bottom surface of the bent Cu) result in significantly increased number density of CuO NWs. Moreover, there is an apparent trend for the tensile stress to result in thicker Cu_2O layer and smaller sizes of grains in both Cu_2O and CuO layers. Such trends suggest that the formation of NWs is intimately related to the growth behavior and microstructures of the underlying CuO and Cu_2O layers.

We have previously shown that CuO nanowires originate directly from individual CuO grains on the intermediate CuO layer, where the facets of CuO grains serve as structure templates for NW nucleation and growth [28]. The crystals grown on different facets are naturally joined together to form a twin or multi-twin structure started from the NW root and continued into the NW along the length direction. Such a growth process thus stipulates an obvious relationship between nanowire density and oxide grain density. For a sample with high nanowire density, we expect a high density of oxide grains as well. The increased density implies expectations of grains with reduced size; this is consistent with our SEM observations.

Since both Cu_2O and CuO are cation-deficient p-type oxides, it has been shown that the oxide growth is controlled via outward diffusion of cations during the oxidation of Cu [30,32–37]. CuO NW growth requires continuous supply of Cu ions from the substrate (i.e., Cu_2O/Cu interface) to the growth tip. For the intermediate range of the oxidation temperature (~300–550 °C) under which oxide NW formation occurs, the atomic flux is dominated by grain boundary diffusion of Cu ions across the Cu_2O and CuO layers. A higher density of grain boundaries within the oxide layers leads to more efficient outward diffusion of Cu ions for CuO NW growth. The promoted CuO NW formation by the in-plane tensile stress can be understood from its effect of the microstructure characteristics of the oxide films formed, which can be strongly influenced by the oxide nucleation and early-stage growth behavior.

Early-stage oxidation of copper has been investigated by *in situ* TEM and the study has revealed that the oxidation typically involves nucleation, growth and coalescence of oxide islands [38–44]. The nucleation of an oxide island on a metal substrate needs to overcome a nucleation barrier E_N, and the number of critical nuclei per unit area is $N_{r^*} = N_0 \exp\left(-\frac{E_N}{kT}\right)$, where N_0 is the number of nucleation sites per unit area of the substrate, k and T are Boltzmann constant and oxidation temperature, respectively. The main contributions to E_N are volume free energy, surface/interfacial free energy, and interfacial strain energy for the formation of an oxide nucleus. By considering heterogeneous nucleation of an oxide island on the metal surface, this activation energy can be obtained as $E_N = f(\theta)\sigma^3 \frac{1}{(\Delta G_V + \Delta G_S)^2}$ [44], where $f(\theta)$ is geometric factor of the surface and interfacial energies, and σ is surface energy of oxide, ΔG_V is the free-energy change that drives the oxidation reaction (i.e., $\Delta G_V < 0$), ΔG_S is strain energy due to the lattice mismatch between the oxide and the metal substrate. A smaller nucleation barrier results in a higher nuclei density of oxide islands.

The volume energy ΔG_V and surface energy σ should remain the same for oxide formation under the different external stresses
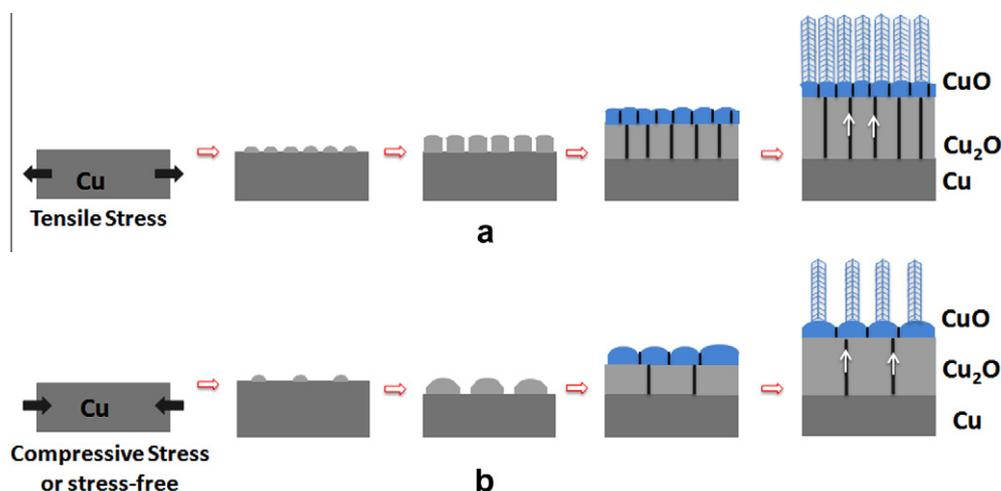

Figure 6. Schematic showing the effect of surface stresses on the microstructure of the oxide layers and the subsequent oxide NW growth, (a) tensile stress; (b) compressive stress or stress-free.

since only Cu_2O is formed initially, i.e., Cu_2O forms as the inner layer in direct contact with the Cu substrate. The strain energy ΔG_S in oxide island due to the lattice mismatch is proportional to $\frac{E}{1-v}\varepsilon^2$ and $\Delta G_S > 0$, where E and v is the Young's modulus and Poisson ratio of Cu_2O, respectively, ε is the lattice mismatch between Cu_2O and the substrate (the lattice constants for Cu and Cu_2O are 3.61 Å and 4.26 Å, respectively). The lattice of the Cu substrate expands under the in-plane tensile stress. Although our samples are polycrystalline Cu, the overall lattice mismatch ε between the oxide and substrate should be reduced by the applied tensile stress. This results in a smaller nucleation activation barrier E_N. Therefore, nucleation of oxide islands is facilitated by the loaded in-plane tensile stress, resulting in a high density of oxide islands on the surface. The lattice mismatch for unbent Cu is large and for in-plane compressive stress becomes even larger, therefore, oxide nuclei on these surfaces have lower densities.

Based on our experimental observations and the early-stage oxidation behaviors described above, the effects of surface bending stresses on the oxide NW growth are schematically shown in Figure 6. Because of the higher density of oxide nuclei enhanced by the tensile stress, as oxidation continues, oxide islands may impinge while still quite small in their lateral size. As a result, the fraction of merged interfaces (i.e., grain boundaries) is effectively increased, which results in a corresponding increase in the effective diffusion rate and total oxide thickness. In addition, the smaller Cu_2O grains leads to finer CuO grains in the top layer, whereby providing more surface sites available for CuO NW nucleation. Since the growth of CuO NWs occurs via the grain boundary diffusion of Cu ions across the Cu_2O and CuO layers, the promoted NW density is a consequence of this enhanced grain boundary diffusion as well as the reduced grain sizes in the CuO layer. For unbent Cu or Cu surface under compression, the average sizes of grains are larger and the fraction of grain boundaries is reduced in comparison to the tensile stress situation. Correspondingly, the total oxide growth including the thickness of the oxide layers and the density of CuO NWs is relatively slow due to the less efficient grain boundary diffusion.

The mechanism shown in Figure 6 stipulates a clear correspondence of the density of CuO NWs with that of the underlying CuO grains. Our preliminary results on Cu foils with different bending curvatures indicate that the NW density increases with increasing the tensile stress by enhancing the oxide nucleation. However, our experimental results show no clear dependence of the diameter and length of CuO NWs with the applied stresses. This is because the diameter of CuO NWs is not defined by the lateral size of the underlying CuO grains. As revealed by our SEM observations, CuO NWs are grown from the top portion of CuO grains [28]. Therefore, the diameter of CuO NWs is smaller than the lateral size of underlying CuO grains, irrespective of the type of surface stresses applied.

5. Conclusion

We have reported the oxidation of bent Cu foils for examining the effect of bending surface stresses on the formation of CuO NWs. In-plane tensile stresses are shown to lead to enhanced oxide NW growth (such as the NW densities) in comparison to in-plane compressive stresses or unbent Cu. These effects are attributed to the effect of tensile stresses on the reduction of lattice mismatch strain between the inner layer of Cu_2O and the Cu substrate, which promotes the nucleation rate of Cu_2O islands and therefore increases the number of grain boundaries formed by impinged small Cu_2O grains. The efficient outward diffusion of Cu ions via an increased number of grain boundaries significantly enhances the CuO NW formation. Our results may have broader impact for fundamental understanding of the mechanisms of metal oxidation and manipulating the gas-surface reaction for effectively promoting oxide NW formation.

References

[1] E. Comini, C. Baratto, G. Faglia, M. Ferroni, A. Vomiero, G. Sberveglieri, Prog. Mater. Sci. 54 (2009) 1.
[2] C.K. Xu, Y.K. Liu, G.D. Xu, G.H. Wang, Mater. Res. Bull. 37 (2002) 2365.
[3] H.-M. Xiao, S.-Y. Fu, L.-P. Zhu, Y.-Q. Li, G. Yang, Eur. J. Inorg. Chem. 1966 (2007).
[4] X.F. Wu, H. Bai, J.X. Zhang, F.E. Chen, G.Q. Shi, J. Phys. Chem. B 109 (2005) 22836.
[5] H. Wu, D.D. Lin, W. Pan, Appl. Phys. Lett. 89 (2006) 133125.
[6] A.A. Umar, M. Oyama, Cryst. Growth Des. 7 (2007) 2404.
[7] Y.Y. Fu, J. Chen, J. Zhang, Chem. Phys. Lett. 350 (2001) 491.
[8] A.M. Goncalves, L.C. Campos, A.S. Ferlauto, R.G. Lacerda, J. Appl. Phys. 106 (2009) 034303.
[9] X.C. Jiang, T. Herricks, Y.N. Xia, Nano Lett. 2 (2002) 1333.
[10] J.T. Chen et al., J. Alloy. Compd. 454 (2008) 268.
[11] N. Chopra, B. Hu, B. Hinds, J. Mater. Res. 22 (2007) 2691.
[12] M. Kaur et al., J. Cryst. Growth 289 (2006) 670.
[13] M. Komatsu, H. Mori, J. Electron Microsc. 54 (2005) 99.
[14] L. Liao et al., Nanotechnology 20 (2009) 085203.
[15] A. Kumar, A.K. Srivastava, P. Tiwari, R.V. Nandedkar, J. Phys.: Condens. Matter 16 (2004) 8531.
[16] A.G. Nasibulin et al., Nano Res. 2 (2009) 373.
[17] Y.H. Sun et al., J. Chem. Phys. 132 (2010) 124705.
[18] C.H. Xu, C.H. Woo, S.Q. Shi, Chem. Phys. Lett. 399 (2004) 62.
[19] X.G. Wen, S.H. Wang, Y. Ding, Z.L. Wang, S.H. Yang, J. Phys. Chem. B 109 (2005) 215.
[20] R.M. Wang, Y.F. Chen, Y.Y. Fu, H. Zhang, C. Kisielowski, J. Phys. Chem. B 109 (2005) 12245.
[21] D.A. Voss, E.P. Bulter, T.E. Michell, Metall. Trans. A 13A (1982) 929.
[22] S. Rachauskas et al., Nanotechnology 20 (2009) 165603.
[23] Y.S. Kim, I.S. Huang, S.J. Kim, C.Y. Lee, J.H. Lee, Sens. Actuators, B 135 (2008) 298.
[24] S.M. Arnold, S.E. Koonce, J. Appl. Phys. 27 (1956) 964.
[25] J.A. Sartell, R.J. Stokes, S.H. Bendel, T.L. Johnson, C.H. Li, Trans. Am. Inst. Mining Metall. Eng. 215 (1959) 420.
[26] B.J. Hansen, G.H. Lu, J.H. Chen, J Nanomater. 2008 (2008) 830474.
[27] B.J. Hansen, H.I. Chan, J. Lu, G.H. Lu, J.H. Chen, Chem. Phys. Lett. 504 (2011) 41.
[28] L. Yuan, Y.Q. Wang, R. Mema, G.W. Zhou, Acta Mater. 59 (2011) 2491.
[29] F. Morin, J. Mater. Sci. Lett. 2 (1983) 383.
[30] Y.F. Zhu, K. Mimura, M. Isshiki, Mater. Trans. 43 (2002) 2173.
[31] M.L. Zhong, D.C. Zeng, Z.W. Liu, H.Y. Yu, X.C. Zhong, W.Q. Qiu, Acta Mater. 58 (2010) 5926.
[32] H.E. Evans, Int. J. Mater. Res. 40 (1995) 1.
[33] R.A. Rapp, Metall. Trans. B 15B (1983) 195.
[34] G.M. Raynaud, R.A. Rapp, Oxid. Met. 21 (1984) 89.
[35] Y. Zhu, K. Mimura, M. Isshiki, Oxid. Met. 62 (2004) 207.
[36] Z. Grzesik, M. Migdalska, Defect Diffus. Forum 289–292 (2009) 429.
[37] Y.F. Zhu, K. Mimura, J.W. Lim, M. Isshiki, Q. Jiang, Metall. and Mat. Trans. A. 37A (2006) 1231.
[38] G.W. Zhou, J.C. Yang, J. Mater. Res. 20 (2005) 1684.
[39] G.W. Zhou, J.C. Yang, Appl. Surf. Sci. 222 (2004) 357.
[40] G.W. Zhou, J.C. Yang, Surf. Sci. 559 (2004) 100.
[41] G.W. Zhou, J.C. Yang, Appl. Surf. Sci. 210 (2003) 165.
[42] G.W. Zhou, J.C. Yang, Surf. Sci. 531 (2003) 359.
[43] G.W. Zhou, J.C. Yang, Phys. Rev. Lett. 89 (2002) 106101.
[44] G.W. Zhou, Appl. Phys. Lett. 94 (2009) 201905.